

Supporting Information

HACA's Heritage: A Free-Radical Pathway to Phenanthrene in Circumstellar Envelopes of Asymptotic Giant Branch Stars

Tao Yang, Ralf I. Kaiser, Tyler P. Troy, Bo Xu, Oleg Kostko, Musahid Ahmed,* Alexander M. Mebel,* Marsel V. Zagidullin, and Valeriy N. Azyazov*

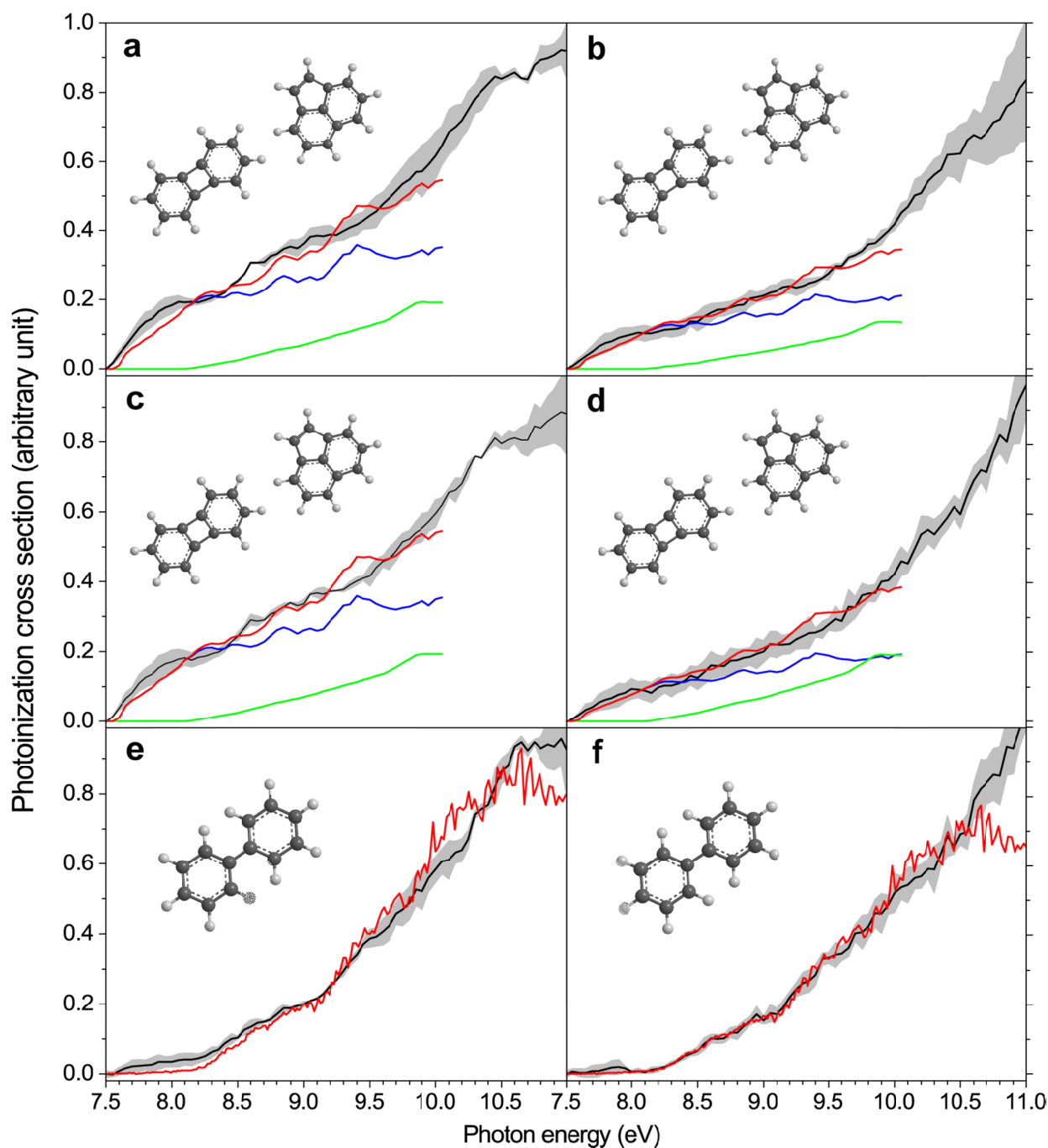
ange_201701259_sm_miscellaneous_information.pdf

Methods

Experimental: The experiments were conducted at the Chemical Dynamics Beamline (9.0.2) of the Advanced Light Source exploiting a resistively-heated silicon-carbide (SiC) high-temperature ‘chemical reactor’ incorporated into a molecular beam apparatus operated with a Wiley-McLaren reflectron time-of-flight mass spectrometer (Re-TOF-MS). The chemical reactor simulates high temperature conditions together with discrete chemical reactions to form PAHs *in situ* through the reaction of radicals. Here, *o*-biphenyl radicals ($C_{12}H_9\cdot$) were prepared at concentrations of less than 0.1 % *in situ* via pyrolysis of the *o*-iodobiphenyl precursor ($C_{12}H_9I$; Sigma Aldrich) seeded in acetylene carrier gas (0.53 ± 0.01 atm; C_2H_2 ; Matheson Gas). The acetylene gas acts as both a carrier and a reactant with the pyrolytically generated radicals. The temperature of the SiC tube was monitored using a Type-C thermocouple and was maintained at $1,500 \pm 10$ K. The reaction products generated in the reactor were expanded supersonically and passed through a 2 mm diameter skimmer located 10 mm downstream of the pyrolytic reactor and into the main chamber, which houses the Re-TOF-MS. The quasi-continuous tunable vacuum ultraviolet (VUV) light from the Advanced Light Source crossed the neutral molecular beam perpendicularly in the extraction region of the RE-TOF-MS. VUV single photon ionization represents essentially a fragment-free ionization technique and hence is classified as a *soft ionization* method compared to electron impact ionization, which results in excessive fragmentation of the parent ion. The ions formed via photoionization are then extracted and impinges onto a microchannel plate detector through an ion lens. Photoionization efficiency (PIE) curves, which report ion counts as a function of photon energy from 7.50 eV to 11.00 eV with a step interval of 0.05 eV at a well-defined mass-to-charge ratio (m/z), were produced by integrating the signal recorded at the specific m/z for the species of interest. Blank experiments were also conducted by expanding neat acetylene carrier gas into the resistively-heated SiC tube without seeding the *o*-iodobiphenyl, and also by helium carrier gas with seeding the *o*-iodobiphenyl. Neither anthracene nor phenanthrene products were observed in these control experiments.

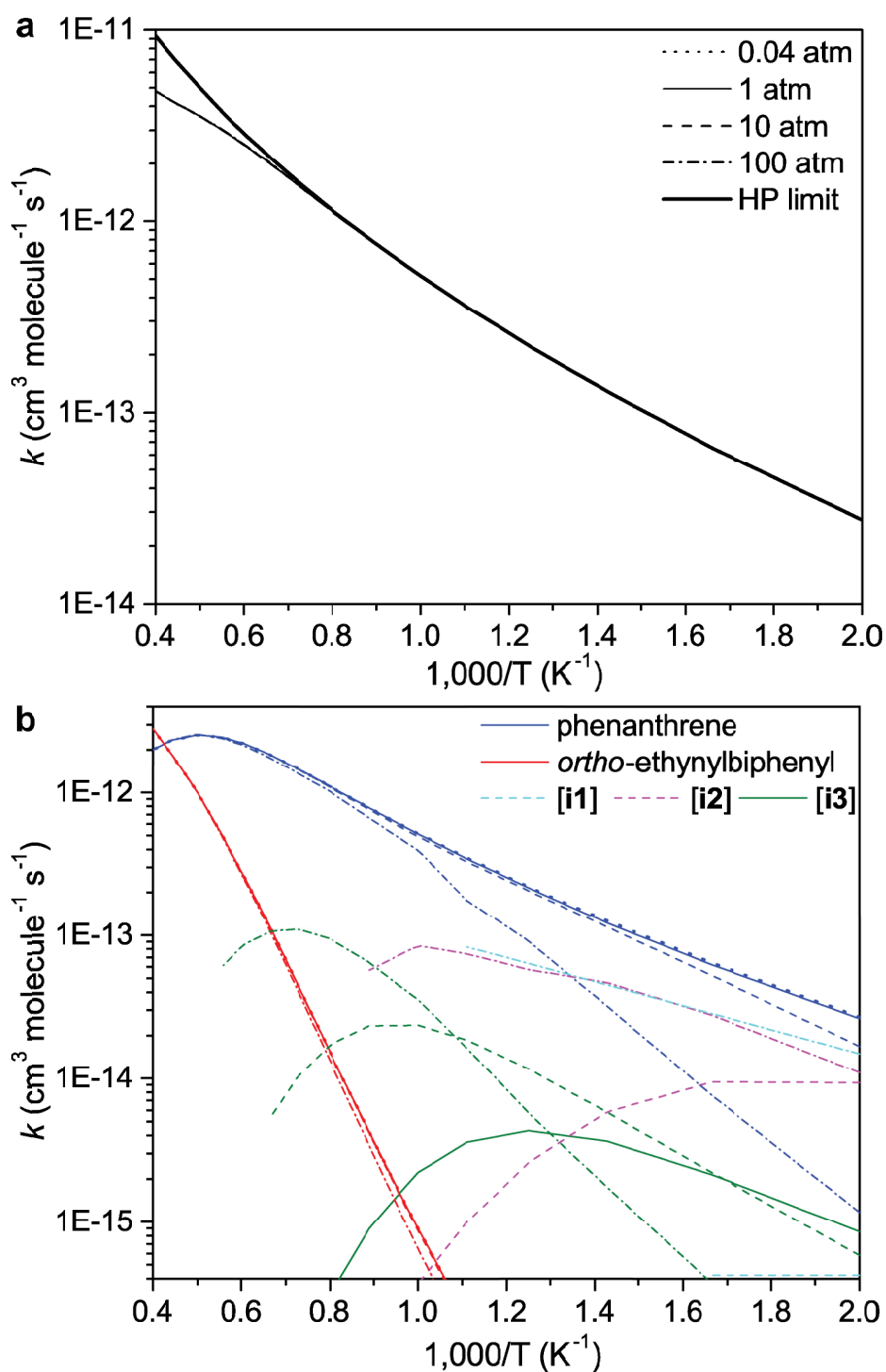
Electronic structure and rate constant calculations: The energies and molecular parameters of various species along the reaction PES were computed at the G3(MP2,CC)//B3LYP/6-311G(d,p) level of theory.^[1-3] This theoretical level is expected to provide bond lengths with accuracy of 0.01-0.02 Å, bond angles within 1-2°, and the energetic parameters of hydrocarbons and their

radicals with ‘chemical accuracy’ within 3-6 kJ mol⁻¹ in terms of average absolute deviations.^[1] The ab initio calculations were performed using the GAUSSIAN 09^[4] and MOLPRO 2010^[5] program packages. Temperature- and pressure-dependent phenomenological rate constants were computed by solving the one-dimensional master equation employing the MESS package.^[6] We used collision parameters derived in the literature for similar systems. Specifically, the Lennard-Jones parameters (ϵ/cm^{-1} , $\sigma/\text{\AA}$), (676.5, 6.31) for biphenyl – an analog of *o*-biphenyl-acetylene – and (101.5, 3.615) for nitrogen were taken from the works by Wang and Frenklach^[7] and Vishnyakov et al.,^[8-9] respectively. Collisional energy transfer in the master equation was described using the “exponential down” model,^[10] with the temperature dependence of the range parameter α for the deactivating wing of the energy transfer function expressed as $\alpha(T) = \alpha_{300}(T/300 \text{ K})^n$, with $n = 0.62$ and $\alpha_{300} = 424 \text{ cm}^{-1}$ calculated earlier for the naphthyl radical (C₁₀H₇) plus argon system, which was shown to be representative for acetylene addition reactions to C₈H₅ and C₈H₇ radicals in argon or nitrogen bath gases.^[11] The Rigid-Rotor, Harmonic-Oscillator (RRHO) model was generally utilized in the calculations of the densities of states and partition functions for the molecular complexes and the number of states for the transition states. Soft normal modes were visually examined and those representing internal rotations were treated as one-dimensional hindered rotors in partition function calculations. Respective one-dimensional torsional potentials were calculated by scanning PESs at the B3LYP/6-311G(d,p) level of theory.



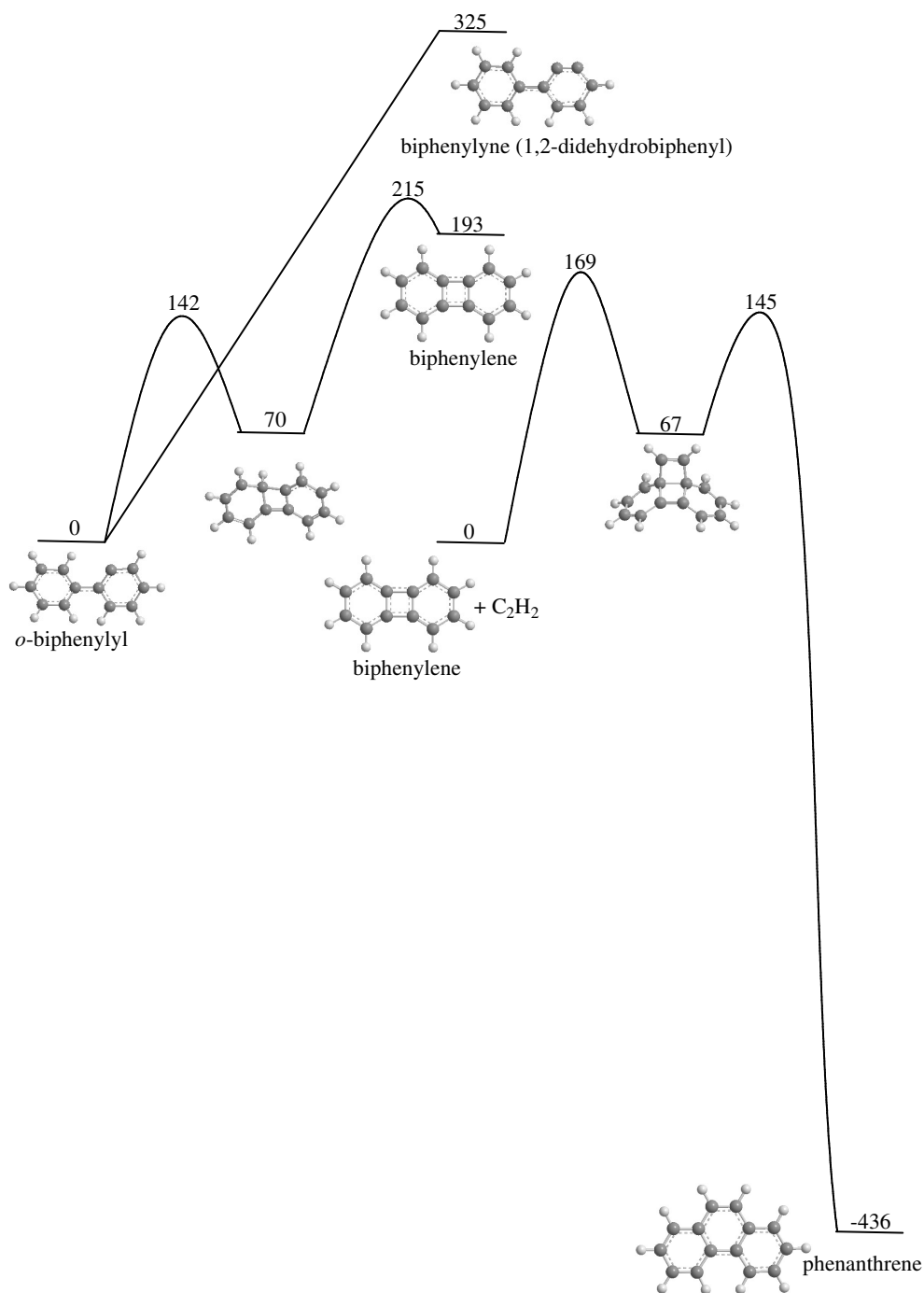
Supplementary Figure 1 | Photoionization efficiency (PIE) curves of various products. The PIE curves were recorded at m/z 152 (a), 153 (c), 154 (e) in the *o*-biphenyl – helium and at m/z 152 (b), 153 (d), 154 (f) in the *o*-biphenyl – acetylene systems. The black lines show the experimental curves with the 1σ error limits defined as the shaded areas. A detailed analysis of the PIEs at m/z 152 to 154 indicates the formation of biphenylene ($C_{12}H_8$; 152 amu; 7.58 ± 0.03

eV^[12-13]) and acenaphthylene (C₁₂H₈; 152 amu; 8.12 ± 0.10^[12-13]), ¹³C-biphenylene and ¹³C-acenaphthylene (¹³CC₁₁H₈; 153 amu), and biphenyl (C₁₂H₁₀; 154 amu; 8.16 ± 0.10^[12-14]). Here, biphenylene is likely formed by hydrogen abstraction from the second aromatic ring of the biphenylyl radical followed by recombination of both radical centers at the *ortho* position of each ring to a four-membered ring leading to biphenylene. Acenaphthalene can be formed via multiple isomerization steps from biphenyl eventually to dihydrocyclopenta[a]indenes (C₁₂H₈) followed by molecular hydrogen loss.^[15] The formation of the biphenyl molecule can be explained by hydrogen abstraction of *o*-biphenylyl from a second *o*-biphenylyl or by atomic hydrogen addition to the *o*-biphenylyl followed by stabilization of the adduct. For **a**, **b**, **c** and **d**, red lines indicate the overall result of the reference PIE curves for biphenylene (C₁₂H₈; blue line)^[12] and acenaphthylene (C₁₂H₈; green line).^[12] For **e** and **f**, the red lines indicate the reference PIE curve for biphenyl (C₁₂H₁₀).^[14] The PIE curves are normalized.



Supplementary Figure 2 | Calculated total (a) and various product formation (b) rate constants (k). The temperature ranges from 500 K to 2,500 K. At various pressures in a, the total rate constants calculated for the different finite pressures are indistinguishable from each other,

and start to merge with the one under the high-pressure (HP) limit when below 1,500 K. In **b**, the line styles are the same as in **a**, and each color represents a single product with various pressures. Notice that lines of phenanthrene at pressures of 0.04 atm (dotted) and 1 atm (thin straight), and the lines of *ortho*-ethynylbiphenyl at pressures of 0.04 atm, 1 atm and 10 atm (dashed) are indistinguishable within the plot range. The lines of **[i1]** at pressures of 0.04 atm and 1 atm, **[i2]** at pressures of 0.04 atm and 1 atm, and **[i3]** at pressure of 0.04 atm are not shown due to their low rate constants. Also in **b**, the case of high-pressure limit is not considered.



Supplementary Figure 3 | Potential energy surfaces for unimolecular decomposition of the *o*-biphenyl radical and for the bimolecular reaction of biphenylene with acetylene. The surfaces are calculated at the G3(MP2,CC)//B3LYP/6-311G(d,p) level of theory. The relative energies are given in kJ mol⁻¹.

Electronic Structure and Statistical Calculations

The calculated PES for unimolecular decomposition of *o*-biphenyl C₁₂H₉ is shown in Supplementary Figure 3. The most favorable dissociation pathway leads to biphenylene via a two-step mechanism involving a four-member ring closure followed by the H atom loss with the overall reaction endoergicity of 193 kJ mol⁻¹ through the highest barrier of 215 kJ mol⁻¹. This pathway appears to be much more preferable than the direct H loss producing biphenylene (1,2-didehydrobiphenyl) endoergic by 325 kJ mol⁻¹. More complex multistep decomposition pathways of *o*-biphenyl to acenaphthalene were mapped out by Shukla et al.³ and were found to have the highest barriers comparable to those for the pathway leading to biphenylene. Considering that the PIE for C₁₂H₈ in the present experiment indicate notably higher contribution of biphenylene than of acenaphthalene, in our RRKM-ME calculations of dissociation rate constants of *o*-biphenyl we focused on the biphenylene formation channel.

Using the calculated rate constants, we evaluated the lifetime of the C₁₂H₉ radical under the conditions in the pyrolytic reactor. At 1,500 K, the computed lifetimes are in the range of 6-13 μs. The modeling results of the conditions in the reactor provided axial residence times in the reactor of 68 to 75 and 112 to 124 μs with acetylene and He as the carrier gases, respectively. Therefore, the C₁₂H₉ radicals that have not reacted with C₂H₂ inside the reactor do not survive and are not observed in the mass spectra. In the meantime, the hydrogen loss from *o*-biphenyl is not instantaneous and in the presence of acetylene this unimolecular reaction is competitive with the bimolecular C₁₂H₉ + C₂H₂ reaction. For instance, considering the pressure of C₂H₂ as 0.04 atm, we evaluate perfect-gas molar concentrations of acetylene as 3.2×10⁻⁷ and 3.5×10⁻⁷ mol cm⁻³ at 1,500 and 1,375 K, respectively. Using the calculated RRKM-ME rate constants for the *o*-biphenyl + C₂H₂ reactions for these conditions, 1.83×10⁻¹² and 1.83×10⁻¹² cm³ molecule⁻¹ s⁻¹, we obtain the pseudo first-order rate constants for the acetylene addition as 3.5×10⁵ and 3.1×10⁵ s⁻¹, which are higher than the rate constants for the unimolecular decomposition of C₁₂H₉, 1.1×10⁵ and 2.8×10⁴ s⁻¹ at 1,500 and 1,375 K, respectively.

Since biphenylene is the major product of unimolecular decomposition of *o*-biphenyl, we investigated the PES for the biphenylene + C₂H₂ reaction (Supplementary Figure 3). Phenanthrene can be produced in two steps via barriers of 169 and 145 kJ mol⁻¹ relative to the initial reactants. These values are much higher than 10 kJ mol⁻¹, the calculated barrier for the C₂H₂ addition to *o*-biphenyl. Rate constants computed for the biphenylene + C₂H₂ →

phenanthrene reaction in the 1,375-1,500 K temperatures range are seven orders of magnitude lower than those for the *o*-biphenyl + C₂H₂ → phenanthrene + H reaction at the same conditions. Clearly, the radical is much more reactive with acetylene than the closed-shell species. The reaction of acenaphthalene (also closed-shell) with C₂H₂ is anticipated to be similarly slow and hence we do not expect that the C₁₂H₈ + C₂H₂ reactions can contribute significantly to the formation of phenanthrene under the experimental conditions.

Modeling Calculations

The residence times of the reactants in the reactor can be modeled via fluid dynamics simulations in the channel of the micro-reactor along with the heat equation for the reactor wall through a detailed evaluation of the pressure and temperature distributions in the reactor based on the solution of the Navier-Stokes equations.^[16] The mass flow rate \dot{M} of the gas is determined by the inlet pressure (initial pressure) $p_0 = 403$ Torr and temperature $T_0 = 300$ K upstream of the choke orifice of a diameter of $d_0 = 0.1$ mm and wall thickness of the plate of $L_0 = 0.5$ mm. Here, the mass flow rate \dot{M} through this choke orifice^[17] is given by equation

$$(S1) \quad \dot{M} = \varphi \pi \left(\frac{d_0}{2}\right)^2 \sqrt{\gamma \left(\frac{2}{\gamma+1}\right)^{\frac{\gamma+1}{\gamma-1}} \frac{p_0}{\sqrt{RT_0}}}$$

Here γ is adiabatic constant, R the ideal gas constant, and φ the discharge coefficient, i.e. the efficient relative fraction of orifice area where gas velocity is equals to sonic velocity. For small thicknesses L , the discharge coefficient ranges from $\varphi = 0.8$ to $\varphi = 0.9$. Our models are conducted with $\varphi = 0.85$. At $p_0 = 403$ Torr and $T_0 = 300$ K, the calculated mass flow rates are determined to be 3.3×10^{-4} g s⁻¹ and 7.7×10^{-4} g s⁻¹ for the He and C₂H₂ carrier gases, respectively. To determine the velocity, pressure, and temperature distributions for the axisymmetric flow, equations S2 to S5 have to be evaluated.^[18]

The mass conservation equation

$$(S2) \quad (\vec{\nabla} \cdot \rho \vec{W}) = 0.$$

Here, \vec{W} represents the gas velocity, ρ the gas density, and $\vec{\nabla}$ the gradient operator.

Momentum conservation equation

$$(S3) \quad \rho(\vec{W} \cdot \vec{\nabla})\vec{W} = -\vec{\nabla}p + (\vec{\nabla} \cdot \mu\vec{\nabla})\vec{W} + \vec{\nabla} \cdot (\mu\vec{\nabla} \vec{W})^T - \frac{2}{3}\vec{\nabla}(\mu\vec{\nabla} \cdot \vec{W}).$$

Here, p is the gas pressure, μ the dynamic viscosity, and $(\mu\vec{\nabla} \vec{W})^T$ the transposed matrix.

Heat transfer equation

$$(S4) \quad \rho C_p(\vec{W} \cdot \vec{\nabla})T + \rho(\vec{W} \cdot \vec{\nabla})\left(\frac{W^2}{2}\right) = (\vec{\nabla}k\vec{\nabla}) + \frac{v}{r}\frac{\partial}{\partial r}\left(\mu r \frac{\partial v}{\partial r}\right).$$

Here k is heat conductivity and C_p the specific heat capacity. The terms in equation (S4) are as follows: the convective heat transfer and convective transfer of kinetic energy respectively along with the molecular energy transfer and work of viscous force. The last term accounts for the z -component of the velocity gradient in radial direction, i.e. $u \ll v, \frac{\partial v}{\partial r} \gg \frac{\partial v}{\partial z}, \frac{\partial u}{\partial z}, \frac{\partial u}{\partial z}$, with u representing the r component of velocity \vec{W} , v the z component of the velocity \vec{W} , r the radial coordinate, and z the axial coordinate. In contrast to Ref. [16], we included in equation (S4) a term with the kinetic gas energy and the work of the viscous force. This modification is important because the gas velocity in regions of reactor is close to the sonic velocity and, hence, the Prandtl number of gas is near unity.

Gas equation

$$(S5) \quad p = \frac{\gamma-1}{\gamma} \rho C_p T.$$

The boundary conditions were exploited for equation (S3) with p_1 as the gas pressure at the entrance of reactor ($z = 0$), p_2 as the gas pressure at the exit of reactor ($z = z_{ex}$), and $V_s = \frac{4l}{4l+d} v_0$ as the gas velocity at the walls of reactor ($r = d/2$).^[19] Here, $l = 1.26\sqrt{\gamma} \frac{\mu}{\rho c_s}$ represents the mean free path, c_s the sonic velocity in the gas, d the internal diameter of reactor, V_s the slip velocity, and v_0 the centerline axial velocity. For equation (S4), we utilized the boundary conditions of the gas temperature $T(z=0) = 300$ K at $z = 0$ and the continuity of the heat flux $q = -k\nabla T$.

To determine the temperature distribution in the walls of silicon carbide tube, the following heat transfer equation for reactor body was employed

$$(S6) \quad -\nabla k_{SiC} \nabla T = Q_R,$$

where k_{SiC} represents the heat conductivity of SiC and Q_R the resistive heat source. Obviously heat source power in section A and C equals zero. The value of Q_R in the section B was varied so that the calculated and measured wall temperatures at the thermocouple installation point coincided. The following boundary conditions was assumed for equation (S6) the temperature at the entrance ($T = 300$ K), the thermal radiation at the exit edge ($-\varepsilon\sigma(T_{ex}^4 - T_0^4)$), the thermal radiation at the outside walls ($-\varepsilon\sigma(T_{wall}^4 - T_0^4)$), and the continuity of the heat flux (inside walls; q_{SiC}). Here, $q_{SiC} = -k_{SiC} \nabla T_{SiC} = q = -k \nabla T$ symbolizes the heat flux on the internal walls, $\varepsilon = 0.85$ the emissivity factor, σ the Stefan–Boltzmann constant, T_{ex} the gas temperature at $z = z_{ex}$, and T_{wall} the temperature of outside wall of SiC tube.

The gas pressure in the chamber, in which the high-temperature chemical micro-reactor was mounted, was extremely low being of the order of a few 10^{-4} Torr. Under these conditions, the local gas velocity at the exit of SiC tube equals the local sonic speed c_s .^[16] Considering the mass flow in our experiment, the gas pressure closer to the exit of the reactor can be less than 10 Torr. Under these conditions, there is slip at the boundaries.^[16, 19] This circumstance is taken into account in the boundary conditions for equation (S3). The temperature dependence of the viscosity, heat conductivity, and heat capacity in the range of $T = 300$ -1,500 K were also considered. Ultimately, all equations were solved using the Comsol Multiphysics package^[20] in 2D axial symmetrical geometry.

The average residence time represents the most important parameter of the reactor. For the interval $[z_1, z_2]$, it is defined via equation

$$(S7) \quad t_a(z_1, z_2) = \int_{z_1}^{z_2} dz \int_0^{\frac{d}{2}} \frac{2\pi r \rho(r, z) dr}{M}.$$

The centerline gas residence time is given by equation

$$(S8) \quad t_c = \int_{z_1}^{z_2} \frac{dz}{v_0},$$

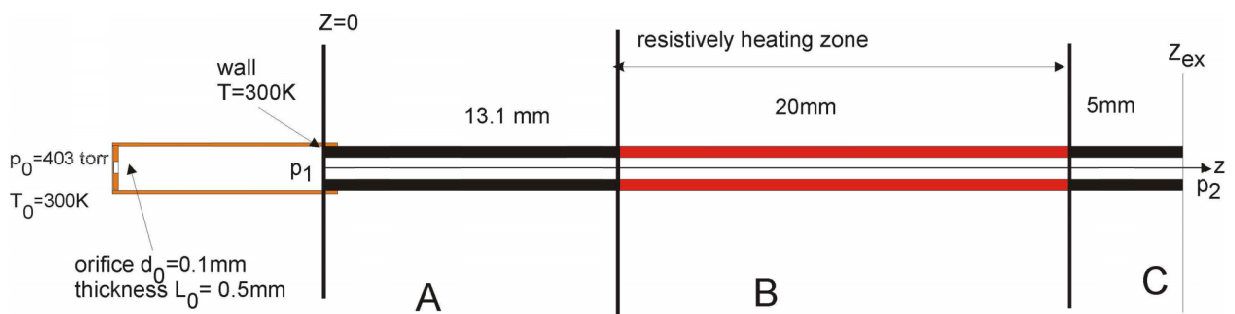
where v_0 is the centerline velocity. The modeled residence times are compiled for helium and acetylene carrier gases in Supplementary Tables 1 and 2.

Supplementary Table 1 | Residence time for helium carrier gas.

Parameter	Interval	Residence time
t_a	$[z_1=13.1, z_2=33.1]$	129 μs
t_c	$[z_1=13.1, z_2=33.1]$	68 μs
t_a	$[z_1=13.1, z_2=38.1]$	142 μs
t_c	$[z_1=13.1, z_2=38.1]$	75 μs

Supplementary Table 2 | Residence time for acetylene carrier gas.

Parameter	Interval, mm	Residence time, μs
t_a	$[z_1=13.1, z_2=33.1]$	212
t_c	$[z_1=13.1, z_2=33.1]$	112
t_a	$[z_1=13.1, z_2=38.1]$	234
t_c	$[z_1=13.1, z_2=38.1]$	124
t_a	$[z_1=22.3, z_2=36.26]$	130



Supplementary Figure 4 | Geometry of the reactor. A and C are unloaded zones and B represents the resistively heated part of SiC tube. Here, p_1 and p_2 are the gas pressure at the entrance ($z=0$) and the exit (z_{ex}) of SiC tube.

References

- [1] L. A. Curtiss, K. Raghavachari, P. C. Redfern, V. Rassolov, J. A. Pople, *J. Chem. Phys.* **1998**, *109*, 7764-7776.
- [2] L. A. Curtiss, K. Raghavachari, P. C. Redfern, A. G. Baboul, J. A. Pople, *Chem. Phys. Lett.* **1999**, *314*, 101-107.
- [3] A. G. Baboul, L. A. Curtiss, P. C. Redfern, K. Raghavachari, *J. Chem. Phys.* **1999**, *110*, 7650.
- [4] M. J. Frisch, G. W. Trucks, H. B. Schlegel, G. E. Scuseria, M. A. Robb, J. R. Cheeseman, G. Scalmani, V. Barone, B. Mennucci, G. A. Petersson *Gaussian 09, Revision A.1*, Gaussian Inc.: Wallingford, CT 06492, U.S.A., **2009**.
- [5] H.-J. Werner, P. J. Knowles, G. Knizia, F. R. Manby, M. Schütz, P. Celani, T. Korona, R. Lindh, A. Mitrushenkov, G. Rauhut *Molpro, Version 2010.1, A Package of Ab Initio Programs*, TTI GmbH: Stuttgart, Germany 70173, **2010**.
- [6] Y. Georgievskii, J. A. Miller, M. P. Burke, S. J. Klippenstein, *J. Phys. Chem. A* **2013**, *117*, 12146-12154.
- [7] H. Wang, M. Frenklach, *Combust. Flame* **1994**, *96*, 163-170.
- [8] A. Vishnyakov, P. G. Debenedetti, A. V. Neimark, *Phys. Rev. E* **2000**, *62*, 538.
- [9] A. V. Neimark, P. I. Ravikovitch, A. Vishnyakov, *Phys. Rev. E* **2000**, *62*, R1493.
- [10] J. Troe, *J. Chem. Phys.* **1977**, *66*, 4745-4757.
- [11] A. M. Mebel, Y. Georgievskii, A. W. Jasper, S. J. Klippenstein, *Proc. Combust. Inst.* **2017**, *36*, 919-926.
- [12] J. Yang, Y. Li, Z. Cheng. *Photoionization Cross Section Database (Version 1.0)*, Accessed on September 16th, 2016, Center for Advanced Combustion and Energy, National Synchrotron Radiation Laboratory, Hefei, Anhui, China (**2011**).
- [13] P. J. Linstrom, W. Mallard, National Institute of Standards and Technology, Gaithersburg MD, 20899, **2001**.
- [14] F. Qi, R. Yang, B. Yang, C. Huang, L. Wei, J. Wang, L. Sheng, Y. Zhang, *Rev. Sci. Instrum.* **2006**, *77*, 084101.
- [15] B. Shukla, K. Tsuchiya, M. Koshi, *J. Phys. Chem. A* **2011**, *115*, 5284-5293.
- [16] Q. Guan, K. N. Urness, T. K. Ormond, D. E. David, G. Barney Ellison, J. W. Daily, *Int. Rev. Phys. Chem.* **2014**, *33*, 447-487.
- [17] L. D. Landau, E. M. Lifshitz, *Fluid Mechanics, Vol. 6*, Butterworth-Heinemann Ltd., Oxford, England, **1987**.
- [18] R. B. Bird, W. E. Stewart, E. N. Lightfoot, *Transport Phenomena*, John Wiley & Sons, Inc., New York, U.S.A., **1960**.
- [19] G. N. Abramovich, *Applied Gas Dynamics*, Nauka Publishing House, Moscow, U.S.S.R., **1969**.
- [20] COMSOL *COMSOL Multiphysics*, COMSOL: Stockholm, Sweden, **2016**.